A hybrid model for modelling arbitrary cracks in isotropic plate structures

Yulin Luo[1,2], Carol A. Featherston[1], David Kennedy[1]*

[1]School of Engineering, Cardiff University, Queens Buildings, The Parade,

Cardiff, CF24 3AA, United Kingdom

[2]State Key Laboratory of Automotive Safety and Energy, Tsinghua University,

Beijing 100084, P.R. China

*Corresponding author. E-mail address: KennedyD@cardiff.ac.uk

Abstract

Damage modelling is essential in preliminary structural design and non-destructive damage detection. This paper investigates changes in natural frequencies of plates due to an arbitrarily aligned crack. A novel hybrid method couples an exact strip model for the intact part with a finite element model for the cracked part. The crack is modelled as a rotational spring with additional rotational freedoms being added to the finite element nodes. The method is validated against published results for through-the-depth cracks. Cracks with varying direction, location, depth and length are used to study the effects of changing the crack parameters.

Keywords: plates, cracks, damage detection, exact strip, finite element, Wittrick-Williams algorithm

1. Introduction

Thin plates and shells are widely used in aerospace and other applications. Plate structural failures can be caused by many factors, such as unexpected loading or environmental conditions leading to defects in the material or damage to the structure, insufficiency in design, and inadequacies in construction or maintenance. Damaged structures can have significantly reduced structural properties leading to sudden failure with potentially catastrophic consequences, including in the worst cases loss of life. This is particularly true for thin-walled structures, where potential instability is a significant factor. For this reason, the ability to detect

damage in terms of localisation and assessment of severity at the very early stages of propagation can enhance the performance and safety of these structures.

Structural performance is degraded by the presence of damage such as cracks, which are often difficult to detect visually, particularly in built-up structures such as wings and fuselage panels [1-6]. Changes in vibration behaviour enable damage to be identified using non-destructive testing techniques, which can be employed with minimal instrumentation if attention is confined to the natural frequencies rather than the vibration modes [7]. By studying changes in either natural frequencies or mode shapes, it is possible to infer the location and severity of damage by comparison with the behaviour of an undamaged structure. This is achieved in two stages, the direct problem and the inverse problem. In the direct problem the effect of damage with a range of severities in different locations is determined. Using this information, the inverse problem is solved to locate and characterise the damage based on changes in vibration behaviour.

The vibration responses of rectangular plates with cracks or singularities under different loading and boundary conditions has been the subject of significant investigation and many methods have been presented to solve this problem. The direction and severity of a crack will impact on both vibrational characteristics and material properties.

A number of studies have been performed to study the effect of cracks running along an axis of symmetry, examples include Stahl and Keer [8], Liew et al. [9], Bose and Mohanty [10], and Huang and Leissa [11] which will be chosen as comparators for the present work. Despite some success, researchers have found it difficult to obtain accurate natural frequency results when the crack extends over the full width of the plate [11] or when its length is small (e.g. less than 20% of the plate width [10]). Stahl and Keer [8] used homogeneous Fredholm integral equations of the second kind to obtain the natural frequencies of a plate with different crack locations. A finite Fourier transform to the differential equation was also used [12-14], with a system of integral equations representing the unknown singularity around the crack. The unknown quantities were expanded into a Fourier series, but the method was limited to the localisation of the crack and to particular boundary conditions of the plate. Qian et al. [15] established a finite element model to investigate the vibration response of a cracked plate. Krawczuk [16] presented a closed form solution formulating the stiffness matrix required to simulate a static through crack in an element to substitue the whole damaged plate. Changes in natural frequencies could be formulated as a function of the length and location of the crack,

the boundary conditions, and the mode shape. Liew et al. [9] applied domain decomposition with the Rayleigh-Ritz method to find the upper bound of natural frequencies for cracked plates. An investigation by Krawczuk et al. [17] on the effect of the plastic zone around a crack on the flexibility of the structure, compared with pure elastic behaviour, demonstrated a rather small influence in contrast to elastic and elasto-plastic crack models. Fujimoto et al. [18] used a hybrid of the finite element method and the body force method to discuss the vibration response of a centrally cracked plate under uniaxial tension. Saito et al. [19] used a finite element model to analyse the linear and nonlinear vibration response of a cantilever plate within a transverse crack. Huang and Leissa [11] used a set of corner functions to simulate the stress singularities and extract the natural frequencies of a plate using the Rayleigh-Ritz method. Their method was extended to thick rectangular plates with arbitrary cracks using Mindlin theory [20].

A relationship was found between the crack orientation and the change in natural frequencies with different boundary conditions having different effects on the vibration response [10, 11]. However, these are two of only a few research studies which describe the effect of changing crack angle on vibration response, most of which studied through-the-depth cracks giving no results for part through-the-depth cracks [11, 21]. Bose and Mohanty [10] incorporated stress theory and strain gradient theory to study the effect of microstructure on vibration response using a modified line spring model, but the changes in natural frequencies obtained from this study were significantly different from those of previous studies [8, 9].

Cracks have been modelled in two different ways: as a reduction in stiffness along the crack path; or by a series of springs added along the crack direction [22-25]. In the first approach, the reduction in stiffness can be represented by a decrease in either cross-sectional area or Young's modulus of the material [26]. Alternatively, spring models simulate the singularity behaviour surrounding a crack by introducing a compliance related to the crack depth. Different relationships have been found experimentally using a strain energy density function based on fracture mechanics theory [27-31].

The crack model used in this paper adopts the second approach, using rotational springs to represent the cracks and adding additional rotational degrees of freedom to the finite elements in the area of damage. The cracks are assumed to be always open. This approach is analogous to that previously applied to beam structures [26, 32], and enables the cracked problem to remain linear. In the cracked elements, the construction of a nodal stiffness matrix

incorporating crack stiffness and the way in which the rotational spring is formulated are an essential part of the present study.

A hybrid model is proposed which couples exact strip analysis for the undamaged part of the plate and finite element analysis for the damaged part as shown in Fig. 1. In the finite element part, a crack is modelled as a rotational spring represented by additional degrees of freedom in the stiffness matrix. The finite element and exact strip dynamic stiffness matrices are assembled into a global dynamic stiffness matrix, using Lagrangian Multipliers to equate the displacements at the boundaries of the two parts. Applying an efficient banded solver for Gauss elimination, the resulting transcendental eigenvalue problem is solved using a modified form of the Wittrick-Williams algorithm [33] for the first few natural frequencies. This novel hybrid cracked plate model, having versatility, accuracy and efficiency, is used to predict the effect of damage on the plate's natural frequencies. These natural frequencies can then be used to solve the inverse problem, by enabling a quantitative relation between the crack parameters and the vibration characteristics to be derived.

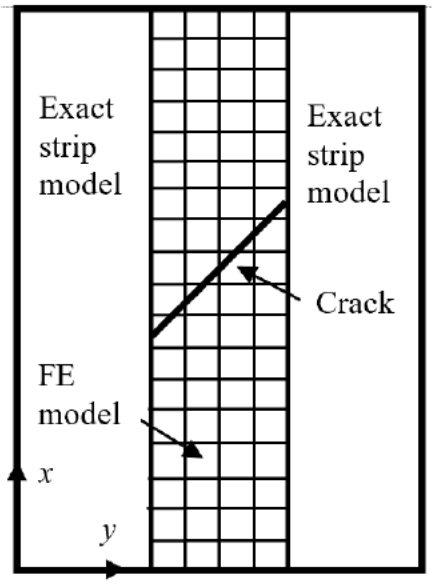

Fig. 1. Hybrid cracked plate model, coupling an exact strip model (ESM) and a finite element (FE) model, with the crack simulated by a rotational spring of stiffness k^*.

The focus in this paper is the direct problem of calculating the changes in natural frequencies of an isotropic simply supported rectangular plate due to a predefined single crack with arbitrary direction, location, depth and length, giving a comprehensive understanding of the relationship between the location and severity of the crack and the free vibration natural frequencies and mode shapes. This study provides a significant advance on other studies where results are commonly restricted to cracks located at the centre or at an edge of the plate, running parallel to the plate edges, over the full length or width, or through the full thickness [8-10]. Section 2 outlines the exact strip and finite element models that are used for the intact and damaged parts of the structure. Section 3 explains how cracks are included in the finite element model. Then in section 4 the two models are combined to form a hybrid model of the whole structure. Section 5 gives numerical results which validate the hybrid model and study the effects of the various crack parameters. Finally, conclusions are presented in section 6.

2. Dynamic stiffness matrices for exact strip and finite element models

The dynamic stiffness method (DSM) provides an efficient, accurate alternative to finite element (FE) analysis by constructing a transcendental stiffness matrix based on exact solutions to the governing differential equations. Such exact solutions require plate structures and their loading to be invariant in the longitudinal (x) direction, so that the vibration or buckling modes can be described by sinusoidal terms in this direction [34]. However, for more complicated structures or arbitrary damage cases, it cannot establish an appropriate model to obtain the vibration characteristics or critical buckling load factors. To balance computational efficiency and the ability to model complex structures, a recent hybrid approach by Suliman et al. [35] extended the capability of the DSM by coupling the exact strip method (ESM) for the intact part of the structure with the more versatile finite element method (FEM) for the damaged part. This approach was used to model delamination damage in composite plates. The present paper further extends the capability of the DSM by coupling the ESM and FEM to enable the modelling of rectangular plates containing cracks of arbitrary length, depth, location and orientation. In contrast to the approach of [35] in which the FEM model had separate nodes for the regions above and below the delaminations, here the finite element mesh is not modified but additional rotational degrees of freedom are assigned to the node of the elements containing cracks.

2.1 Exact strip model

DSM is well established and has been incorporated into a range of software giving exact formulations for beam-like structures [36]. The elements of the dynamic stiffness matrix are highly transcendental functions of the frequency and so lead to a nonlinear eigenvalue problem, preventing the use of standard linear eigensolvers to extract the natural frequencies and critical buckling loads. Wittrick and Williams [33] proposed an efficient and accurate algorithm that gives all required natural frequencies below a chosen trial frequency to any desired accuracy. ESM is an extension of DSM for plate-like structures which was first presented by Wittrick [37], and is based on obtaining explicit closed form solutions to the governing differential equations. Plates are divided where necessary into a series of strips which are rigidly connected along their longitudinal edges. The mode shape is assumed to vary sinusoidally in the longitudinal direction, with any spatial phase differences in the forces and displacements handled by using complex arithmetic. For the common cases of isotropic, orthotropic and symmetrically layered composite plates, the displacements are decoupled into out-of-plane and in-plane systems [37]. For each strip, separate stiffness matrices are defined for these two systems, and it is noted that the lowest natural frequencies are always obtained from the out-of-plane system. This paper only considers the out-of-plane system, which is sufficient to illustrate the proposed hybrid method and to make comparisons with results from the literature.

As shown in Fig. 1, an ESM model is chosen for the intact portion of the plate and the assumption of sinusoidal variation enables the plate structure to be reduced from a two-dimensional to a one-dimensional element through a dynamic stiffness matrix. Software adopting this approach includes VIPASA [34], and its extension VICON [38, 39] which handles the skewed mode shapes arising from shear loading or anisotropy by the introduction of Lagrangian multipliers to couple sinusoidal responses with different half-wavelengths λ. The VICON stiffness equations can be expressed as [39]

$$\begin{bmatrix} l\mathbf{K}_1 & \mathbf{0} & \mathbf{0} & \cdots & \mathbf{0} & \mathbf{E}_1^{\mathrm{H}} \\ \mathbf{0} & l\mathbf{K}_2 & \mathbf{0} & \cdots & \mathbf{0} & \mathbf{E}_2^{\mathrm{H}} \\ \mathbf{0} & \mathbf{0} & l\mathbf{K}_3 & \cdots & \mathbf{0} & \mathbf{E}_3^{\mathrm{H}} \\ \vdots & \vdots & \vdots & \ddots & \vdots & \vdots \\ \mathbf{0} & \mathbf{0} & \mathbf{0} & \mathbf{0} & l\mathbf{K}_j & \mathbf{E}_j^{\mathrm{H}} \\ \mathbf{E}_1 & \mathbf{E}_2 & \mathbf{E}_3 & \cdots & \mathbf{E}_j & \mathbf{0} \end{bmatrix} \begin{bmatrix} \mathbf{D}_1 \\ \mathbf{D}_2 \\ \mathbf{D}_3 \\ \vdots \\ \mathbf{D}_j \\ \mathbf{P}_L \end{bmatrix} = \begin{bmatrix} \mathbf{P}_1 \\ \mathbf{P}_2 \\ \mathbf{P}_3 \\ \vdots \\ \mathbf{P}_j \\ \mathbf{0} \end{bmatrix} \tag{1}$$

where $\mathbf{K}_1, \mathbf{K}_2, \ldots, \mathbf{K}_j$ are the ESM (VIPASA) stiffness matrices derived in [34] using classical plate theory for sinusoidal variation with half-wavelengths $\lambda_1, \lambda_2, \ldots, \lambda_j$ and $\mathbf{D}_1, \mathbf{D}_2, \ldots, \mathbf{D}_j$ are the corresponding displacement vectors; $\mathbf{E}_1, \mathbf{E}_2, \ldots, \mathbf{E}_j$ are constraint matrices used to enforce the longitudinal end conditions; and $\mathbf{P}_L$ is the vector of Lagrangian Multipliers. $\mathbf{P}_1, \mathbf{P}_2, \ldots, \mathbf{P}_j$ are random force vectors, while l is the length of the plate and H denotes the Hermitian transpose.

2.2 Finite element model

Classical plate theory is also used in the finite element model used for the damaged part of the plate. This region is divided into identical rectangular elements with four nodes and three out-of-plane degrees of freedom per node, namely out-of-plane displacement w and rotations θ_x and θ_y about the x and y axes, respectively, see Fig. 1. The static stiffness matrix $\mathbf{k}$ and mass matrix $\mathbf{m}$ for individual undamaged elements are taken from Przemieniecki [40] in the form

$$\mathbf{k} = \begin{bmatrix} \mathbf{k}_{11} & \mathbf{k}_{12} & \mathbf{k}_{13} & \mathbf{k}_{14} \\ \mathbf{k}_{21} & \mathbf{k}_{22} & \mathbf{k}_{23} & \mathbf{k}_{24} \\ \mathbf{k}_{31} & \mathbf{k}_{32} & \mathbf{k}_{33} & \mathbf{k}_{34} \\ \mathbf{k}_{41} & \mathbf{k}_{42} & \mathbf{k}_{43} & \mathbf{k}_{44} \end{bmatrix} \quad , \quad \mathbf{m} = \begin{bmatrix} \mathbf{m}_{11} & \mathbf{m}_{12} & \mathbf{m}_{13} & \mathbf{m}_{14} \\ \mathbf{m}_{21} & \mathbf{m}_{22} & \mathbf{m}_{23} & \mathbf{m}_{24} \\ \mathbf{m}_{31} & \mathbf{m}_{32} & \mathbf{m}_{33} & \mathbf{m}_{34} \\ \mathbf{m}_{41} & \mathbf{m}_{42} & \mathbf{m}_{43} & \mathbf{m}_{44} \end{bmatrix} \tag{2}$$

$$\mathbf{K}_{\mathrm{FE}} = \mathbf{K} + \omega^2 \mathbf{M} \tag{3}$$

where ω is the frequency of vibration.

3. Crack modelling

In the hybrid VICON and FE method (VFM) of this paper, the ESM (VICON) model of section 2.1 is used for the undamaged parts of the structure, while the FE model of section 2.2 is used for the damaged parts. Section 3 describes how damage is introduced to the FE model, in the form of an arbitrarily located and aligned crack extending part way through the thickness of the plate.

3.1 Rotational spring model

A concentrated open crack in a flat thin plate can be represented by a rotational spring of stiffness k^* about the crack direction as shown in Fig. 1. In a manner analogous to that used for modelling cracks in beams [26, 32, 41], the spring stiffness k^* is assumed to be related to the crack depth d by

$$k^* = \frac{D}{b} \times \frac{1}{\lambda^*} \tag{4}$$

in which

$$\lambda^* = \frac{h}{b} \times C\,(d/h) \tag{5}$$

where λ^* is the dimensionless local compliance, b is the width of the plate, h is its thickness and D is its flexural rigidity. $C(d/h)$ is a dimensionless function that can be generalised as [26]

$$C(d/h) = \frac{(d/h)[2-(d/h)]}{0.9[1-(d/h)]^2} \tag{6}$$

For crack simulation in plate elements, it is convenient to use the depth-dependent compliance

$$C^* = \frac{1}{k^*} \tag{7}$$

instead of the stiffness itself to avoid any singularities occurring during the calculation. The rotational compliances associated with the crack are determined prior to their being allocated to their respective element nodes and thus incorporated into the element stiffness matrices and hence the global stiffness matrix.

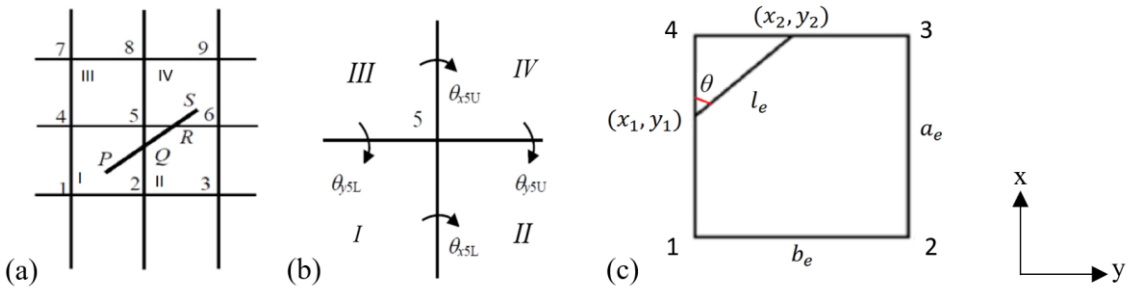

Fig. 2 (a) Detail of the FE portion of VFM model; (b) Rotational degrees of freedom at node 5 of the cracked portion; (c) An example of arbitrary cracked element extracted from the FE portion.

3.2 Crack modelling for plate elements

Consider the longitudinal damaged portion of the plate containing the crack as shown in Fig. 1. Suppose the crack runs along the line *PQRS* shown in Fig. 2(a), passing through the elements numbered I, II and IV. The crack has a depth dependent compliance $\overline{\overline{C^*}}$ per unit length [29], which is resolved into rotational components $\overline{\overline{C_x^*}}$ and $\overline{\overline{C_y^*}}$ about the *x* and *y* axes, respectively. The components in element I are integrated along *PQ* using shape functions to allocate the resulting compliances ($C_{xi}^*, C_{yi}^*; i = 1,2,4,5$) to nodes (1, 2, 4, 5), respectively. Similar allocation of the compliances occurring along *QR* in element II and along *RS* in element IV are made to nodes (2, 3, 5, 6) and (5, 6, 8, 9), respectively.

The intact FE model has three degrees of freedom at each node *i*: out-of-plane displacement *w* and rotations θ_{xi} and θ_{yi} about the *x* and *y* axes, respectively. Nodes to which rotational compliances (C_{xi}^*, C_{yi}^*) have been allocated (e.g. node 5 in Fig. 2(b)) have different rotations ($\theta_{xi\mathrm{L}}, \theta_{xi\mathrm{U}}$) and $\left(\theta_{yi\mathrm{L}}, \theta_{yi\mathrm{U}}\right)$ either side of the node, so that the number of degrees of freedom is increased from 3 to 5. The elements meeting at node 5 each connect to the appropriate degrees of freedom, e.g. element I connects to ($w_5, \theta_{x5L}, \theta_{y5L}$) while element II connects to ($w_5, \theta_{x5L}, \theta_{y5U}$), and so on. Rotational springs of stiffness ($1/C_{x5}^*$, $1/C_{y5}^*$) connect the degrees of freedom ($\theta_{x5L}, \theta_{x5U}$) and ($\theta_{y5L}, \theta_{y5U}$), respectively. Note that the out-of-plane displacement w_5 does not change across the node because the crack is assumed to extend only part way through the plate thickness.

Details of the above calculations will now be given for a typical cracked element, shown in Fig. 2(c). Within this element the crack runs between the points (x_1, y_1) and (x_2, y_2), which can lie either on the boundaries of the element or in its interior. The crack is aligned at a clockwise angle

$$\theta = \tan^{-1}\left(\frac{y_2 - y_1}{x_2 - x_1}\right) \tag{8}$$

to the *x* axis and extends over a length

$$l_e = \sqrt{(x_2 - x_1)^2 + (y_2 - y_1)^2} \tag{9}$$

within the element. By analogy with crack models for beam-like structures, the rotational compliance per unit length about each axis is given as

$$\overline{C_x^*} = (C^* \cos\theta)/a_e \quad , \quad \overline{C_y^*} = (C^* \sin\theta)/b_e \tag{10}$$

where the element dimensions (a_e, b_e) are shown in Fig. 2(c). Then, the compliance per unit length per element is given by

$$\overline{\overline{C_x^*}} = \overline{C_x^*}/a_e \quad , \quad \overline{\overline{C_y^*}} = \overline{C_y^*}/b_e \tag{11}$$

Compliances (C_{xi}^*, C_{yi}^*) at each node of the element are obtained by integration along the crack direction using a set of shape functions, so that

$$C_{xi}^* = \int_0^{l_e} N_i(x,y)\, \overline{\overline{C_x^*}}\, dl \quad , \quad C_{yi}^* = \int_0^{l_e} N_i(x,y)\, \overline{\overline{C_y^*}}\, dl \tag{12}$$

where the shape functions are given by

$$\begin{aligned} N_1 &= \left(1 - \frac{x}{a_e}\right)\left(1 - \frac{y}{b_e}\right) \quad , \quad N_2 = \left(1 - \frac{x}{a_e}\right)\left(\frac{y}{b_e}\right) \\ N_3 &= \left(\frac{x}{a_e}\right)\left(\frac{y}{b_e}\right) \quad , \quad N_4 = \left(\frac{x}{a_e}\right)\left(1 - \frac{y}{b_e}\right) \end{aligned} \tag{13}$$

In order to perform the integrations in Eq. (12)), dl is replaced for each axis by

$$dx = (\cos\theta)dl \quad , \quad dy = (\sin\theta)dl \tag{14}$$

where

$$y = y_1 + (x - x_1)\tan\theta \quad , \quad x = x_1 + (y - y_1)\cot\theta \tag{15}$$

Therefore, substituting Eqs. (14)) and (15)) into Eq. (12)), the additional rotational compliances at the nodes become

$$C_{xi}^* = \int_{x_1}^{x_2} \frac{h\, C(d/h)\, N_i(x,y)}{D\, a_e^2}\, dx \quad , \quad C_{yi}^* = \int_{y_1}^{y_2} \frac{h\, C(d/h)\, N_i(x,y)}{D\, b_e^2}\, dy \tag{16}$$

With the nodal sequence shown in Fig. 2(c), the integrals of Eq. (16) are evaluated as

$$\begin{aligned} C_{x1}^* = \frac{h\, C(d/h)}{D\, a_e^3 b_e} \Bigg\{ & [a_e x_1 \tan\theta + a_e(b_e - y_1)](x_2 - x_1) \\ & - [(a_e + x_1)\tan\theta + (b_e - y_1)]\left(\frac{x_2^2 - x_1^2}{2}\right) \\ & + \tan\theta\left(\frac{x_2^3 - x_1^3}{3}\right)\Bigg\} \end{aligned} \tag{17}$$

$$C^*_{x2} = \frac{h\,C(d/h)}{D\,a_e^3 b_e}\left\{[-a_e x_1 \tan\theta + a_e y_1](x_2 - x_1) + [(a_e + x_1)\tan\theta - y_1]\left(\frac{x_2^2 - x_1^2}{2}\right) - \tan\theta\left(\frac{x_2^3 - x_1^3}{3}\right)\right\}$$

$$C^*_{x3} = \frac{h\,C(d/h)}{D\,a_e^3 b_e}\left\{[-x_1 \tan\theta + y_1]\left(\frac{x_2^2 - x_1^2}{2}\right) + \tan\theta\left(\frac{x_2^3 - x_1^3}{3}\right)\right\}$$

$$C^*_{x4} = \frac{h\,C(d/h)}{D\,a_e^3 b_e}\left\{[x_1 \tan\theta + (b_e - y_1)]\left(\frac{x_2^2 - x_1^2}{2}\right) - \tan\theta\left(\frac{x_2^3 - x_1^3}{3}\right)\right\}$$

$$C^*_{y1} = \frac{h\,C(d/h)}{D\,a_e b_e^3}\left\{[b_e(a_e - x_1) + b_e y_1 \cot\theta](y_2 - y_1) - [(a_e - x_1) + (b_e + y_1)\cot\theta]\left(\frac{y_2^2 - y_1^2}{2}\right) + \cot\theta\left(\frac{y_2^3 - y_1^3}{3}\right)\right\}$$

$$C^*_{y2} = \frac{h\,C(d/h)}{D\,a_e b_e^3}\left\{[(a_e - x_1) + y_1 \cot\theta]\left(\frac{y_2^2 - y_1^2}{2}\right) - \cot\theta\left(\frac{y_2^3 - y_1^3}{3}\right)\right\}$$

$$C^*_{y3} = \frac{h\,C(d/h)}{D\,a_e b_e^3}\left\{[x_1 - y_1 \cot\theta]\left(\frac{y_2^2 - y_1^2}{2}\right) + \cot\theta\left(\frac{y_2^3 - y_1^3}{3}\right)\right\}$$

$$C^*_{y4} = \frac{h\,C(d/h)}{D\,a_e b_e^3}\left\{[b_e x_1 - b_e y_1 \cot\theta](y_2 - y_1) + [-x_1 + (b_e + y_1)\cot\theta]\left(\frac{y_2^2 - y_1^2}{2}\right) - \cot\theta\left(\frac{y_2^3 - y_1^3}{3}\right)\right\}$$

The 27×27 global static stiffness matrix for the four elements shown in Fig. 2(a) is assembled as

$$\mathbf{K} = \mathbf{k} + \mathbf{k}^* \tag{18}$$

where $\mathbf{k}$ is formed in the usual way, temporarily ignoring the effects of the crack, i.e.

$$\mathbf{k} = \begin{bmatrix}
\mathbf{k}^{\mathrm{I}}_{11} & \mathbf{k}^{\mathrm{I}}_{12} & \mathbf{0} & \mathbf{k}^{\mathrm{I}}_{14} & \mathbf{k}^{\mathrm{I}}_{13} & \mathbf{0} & \mathbf{0} & \mathbf{0} & \mathbf{0} \\
\mathbf{k}^{\mathrm{I}}_{21} & \mathbf{k}^{\mathrm{I}}_{22} + \mathbf{k}^{\mathrm{II}}_{11} & \mathbf{k}^{\mathrm{II}}_{12} & \mathbf{k}^{\mathrm{I}}_{24} & \mathbf{k}^{\mathrm{I}}_{23} + \mathbf{k}^{\mathrm{II}}_{14} & \mathbf{k}^{\mathrm{II}}_{13} & \mathbf{0} & \mathbf{0} & \mathbf{0} \\
\mathbf{0} & \mathbf{k}^{\mathrm{II}}_{21} & \mathbf{k}^{\mathrm{II}}_{22} & \mathbf{0} & \mathbf{k}^{\mathrm{II}}_{24} & \mathbf{k}^{\mathrm{II}}_{23} & \mathbf{0} & \mathbf{0} & \mathbf{0} \\
\mathbf{k}^{\mathrm{I}}_{41} & \mathbf{k}^{\mathrm{I}}_{42} & \mathbf{0} & \mathbf{k}^{\mathrm{I}}_{44} + \mathbf{k}^{\mathrm{III}}_{11} & \mathbf{k}^{\mathrm{I}}_{43} + \mathbf{k}^{\mathrm{III}}_{12} & \mathbf{0} & \mathbf{k}^{\mathrm{III}}_{14} & \mathbf{k}^{\mathrm{III}}_{13} & \mathbf{0} \\
\mathbf{k}^{\mathrm{I}}_{31} & \mathbf{k}^{\mathrm{I}}_{32} + \mathbf{k}^{\mathrm{II}}_{41} & \mathbf{k}^{\mathrm{II}}_{42} & \mathbf{k}^{\mathrm{I}}_{34} + \mathbf{k}^{\mathrm{III}}_{21} & \mathbf{k}^{\mathrm{I}}_{33} + \mathbf{k}^{\mathrm{II}}_{44} + \mathbf{k}^{\mathrm{III}}_{22} + \mathbf{k}^{\mathrm{IV}}_{11} & \mathbf{k}^{\mathrm{II}}_{43} + \mathbf{k}^{\mathrm{IV}}_{12} & \mathbf{k}^{\mathrm{III}}_{24} & \mathbf{k}^{\mathrm{III}}_{23} + \mathbf{k}^{\mathrm{IV}}_{14} & \mathbf{k}^{\mathrm{IV}}_{13} \\
\mathbf{0} & \mathbf{k}^{\mathrm{II}}_{31} & \mathbf{k}^{\mathrm{II}}_{32} & \mathbf{0} & \mathbf{k}^{\mathrm{II}}_{34} + \mathbf{k}^{\mathrm{IV}}_{21} & \mathbf{k}^{\mathrm{II}}_{33} + \mathbf{k}^{\mathrm{IV}}_{22} & \mathbf{0} & \mathbf{k}^{\mathrm{IV}}_{24} & \mathbf{k}^{\mathrm{IV}}_{23} \\
\mathbf{0} & \mathbf{0} & \mathbf{0} & \mathbf{k}^{\mathrm{III}}_{41} & \mathbf{k}^{\mathrm{III}}_{42} & \mathbf{0} & \mathbf{k}^{\mathrm{III}}_{44} & \mathbf{k}^{\mathrm{III}}_{43} & \mathbf{0} \\
\mathbf{0} & \mathbf{0} & \mathbf{0} & \mathbf{k}^{\mathrm{III}}_{31} & \mathbf{k}^{\mathrm{III}}_{32} + \mathbf{k}^{\mathrm{IV}}_{41} & \mathbf{k}^{\mathrm{IV}}_{42} & \mathbf{k}^{\mathrm{III}}_{34} & \mathbf{k}^{\mathrm{III}}_{33} + \mathbf{k}^{\mathrm{IV}}_{44} & \mathbf{k}^{\mathrm{IV}}_{43} \\
\mathbf{0} & \mathbf{0} & \mathbf{0} & \mathbf{0} & \mathbf{k}^{\mathrm{IV}}_{31} & \mathbf{k}^{\mathrm{IV}}_{32} & \mathbf{0} & \mathbf{k}^{\mathrm{IV}}_{34} & \mathbf{k}^{\mathrm{IV}}_{33}
\end{bmatrix} \tag{19}$$

In Eq. (19) each $\mathbf{k}_{ij}^{e}$ is a 3×3 portion of the stiffness matrix for element e relating the forces at node i to the displacements at node j, as numbered in Fig. 2(c). $\mathbf{k}^{*}$ is a matrix containing the rotational spring stiffness to be added at all nodes belonging to elements which contain a crack, i.e. in all nodes except node 7. These nodes are given additional degrees of freedom, and the rotational freedoms are connected by rotational spring stiffnesses generated from the nodal compliances due to the presence of the crack in elements I , II, and IV. For example, each of these elements provides rotational springs which connect the degrees of freedom $(w_5, \theta_{x5\mathrm{L}}, \theta_{x5\mathrm{U}}, \theta_{y5\mathrm{L}}, \theta_{y5\mathrm{U}})$ at node 5 by

$$\mathbf{k}_5^{*} = \begin{bmatrix} 0 & & & 0 & & \\ & {}^{1}/_{C_{x5}^{*}} & & -{}^{1}/_{C_{x5}^{*}} & & \\ & & {}^{1}/_{C_{y5}^{*}} & & -{}^{1}/_{C_{y5}^{*}} & \\ 0 & & & 0 & & \\ & -{}^{1}/_{C_{x5}^{*}} & & {}^{1}/_{C_{x5}^{*}} & & \\ & & -{}^{1}/_{C_{y5}^{*}} & & {}^{1}/_{C_{y5}^{*}} & \end{bmatrix} \tag{20}$$

The total contribution of rotational springs to the 9 nodes is given by

$$\mathbf{k}^{*} = \begin{bmatrix} \mathbf{k}_1^{*\mathrm{I}} & \mathbf{0} & \mathbf{0} & \mathbf{0} & \mathbf{0} & \mathbf{0} & \mathbf{0} & \mathbf{0} & \mathbf{0} \\ \mathbf{0} & \mathbf{k}_2^{*\mathrm{I}} + \mathbf{k}_2^{*\mathrm{II}} & \mathbf{0} & \mathbf{0} & \mathbf{0} & \mathbf{0} & \mathbf{0} & \mathbf{0} & \mathbf{0} \\ \mathbf{0} & \mathbf{0} & \mathbf{k}_3^{*\mathrm{II}} & \mathbf{0} & \mathbf{0} & \mathbf{0} & \mathbf{0} & \mathbf{0} & \mathbf{0} \\ \mathbf{0} & \mathbf{0} & \mathbf{0} & \mathbf{k}_4^{*\mathrm{I}} & \mathbf{0} & \mathbf{0} & \mathbf{0} & \mathbf{0} & \mathbf{0} \\ \mathbf{0} & \mathbf{0} & \mathbf{0} & \mathbf{0} & \mathbf{k}_5^{*\mathrm{I}} + \mathbf{k}_5^{*\mathrm{II}} + \mathbf{k}_5^{*\mathrm{IV}} & \mathbf{0} & \mathbf{0} & \mathbf{0} & \mathbf{0} \\ \mathbf{0} & \mathbf{0} & \mathbf{0} & \mathbf{0} & \mathbf{0} & \mathbf{k}_6^{*\mathrm{II}} + \mathbf{k}_6^{*\mathrm{IV}} & \mathbf{0} & \mathbf{0} & \mathbf{0} \\ \mathbf{0} & \mathbf{0} & \mathbf{0} & \mathbf{0} & \mathbf{0} & \mathbf{0} & \mathbf{0} & \mathbf{0} & \mathbf{0} \\ \mathbf{0} & \mathbf{0} & \mathbf{0} & \mathbf{0} & \mathbf{0} & \mathbf{0} & \mathbf{0} & \mathbf{k}_8^{*\mathrm{IV}} & \mathbf{0} \\ \mathbf{0} & \mathbf{0} & \mathbf{0} & \mathbf{0} & \mathbf{0} & \mathbf{0} & \mathbf{0} & \mathbf{0} & \mathbf{k}_9^{*\mathrm{IV}} \end{bmatrix} \tag{21}$$

The equivalent dynamic stiffness matrix for the FE part is given by Eq. (3). Note that the mass matrix is assembled in the same way as **k** in Eq. (19), the crack having no effect on it because it is assumed to cause no reduction in the mass of the plate.

4. Hybrid VFM model

As mentioned earlier, the hybrid VFM model for modelling arbitrarily located and aligned cracks has been developed from a method proposed by Suliman et al. [35] to model the effect of delamination in composite plates. The rectangular plate is divided into two parts, as shown

in Fig. 1, the cracked part being modelled by FE coupled with ESM for the intact part. The displacements and rotations at the boundaries are constrained to be equal by Lagrangian multipliers. The natural frequencies are determined by the Wittrick-Williams algorithm [33], while mode shapes are obtained by a random force vector method proposed by Hopper and Williams [42]. The hybrid dynamic stiffness matrix is assembled as

$$\mathbf{K}_{\mathrm{VFM}} = \begin{bmatrix} \mathbf{K}_{\mathrm{GV}} & \mathbf{0} & \mathbf{C}_1{}^{\mathrm{H}} \\ \mathbf{0} & \mathbf{K}_{\mathrm{FE}} & \mathbf{C}_2{}^{\mathrm{T}} \\ \mathbf{C}_1 & \mathbf{C}_2 & \mathbf{0} \end{bmatrix} \tag{22}$$

in which $\mathbf{K}_{\mathrm{GV}}$ is the portion of the global ESM stiffness matrix in Eq. (1) including uncoupled VIPASA stiffness matrices associated with sinusoidal modes with different half-wavelengths

$$\mathbf{K}_{\mathrm{GV}} = \begin{bmatrix} l\mathbf{K}_1 & \mathbf{0} & \mathbf{0} & \cdots & \mathbf{0} \\ \mathbf{0} & l\mathbf{K}_2 & \mathbf{0} & \cdots & \mathbf{0} \\ \mathbf{0} & \mathbf{0} & l\mathbf{K}_3 & \cdots & \mathbf{0} \\ \vdots & \vdots & \vdots & \ddots & \vdots \\ \mathbf{0} & \mathbf{0} & \mathbf{0} & \mathbf{0} & l\mathbf{K}_j \end{bmatrix} \tag{23}$$

$\mathbf{K}_{\mathrm{FE}}$ is the hybrid FE dynamic stiffness matrix of Eq. (3) after application of the crack through the analysis of Section 3, while $\mathbf{C}_1$ and $\mathbf{C}_2$ are constraint matrices that enforce equal displacement and rotations at the boundaries between the intact and damaged parts of the plate. $\mathbf{C}_1$ also contains any point support conditions of the intact part. From Eq. (1),

$$\mathbf{C}_1 = [\mathbf{E}_1 \quad \mathbf{E}_2 \quad \mathbf{E}_3 \quad \cdots \quad \mathbf{E}_j] \tag{24}$$

T denotes the transpose of a matrix and H denotes the Hermitian transpose.

4.1 Banded Gauss elimination in Wittrick-Williams algorithm

Computational efficiency is an important consideration in damage detection and the related forward problem due to the large number of simulations which need to be performed. ESM can significantly enhance the efficiency of modelling the effect of damage on the vibration characteristics of a structure by avoiding discretisation into elements, with the Wittrick-Williams algorithm providing exact solutions for the resulting transcendental eigenvalue problem. However, it can only be applied directly to prismatic structures, and the presence of an arbitrary crack is handled by the hybrid VFM method introduced in this paper. Here the

computational time significantly increases, even when using a powerful computer, and is dominated by the Gauss elimination operations required by the Wittrick-Williams algorithm.

From Eqs. (22)-(24), the matrix to be triangulated has the form [39]

$$\mathbf{K}_{\mathrm{VFM}} = \begin{bmatrix} l\mathbf{K}_1 & \mathbf{0} & \mathbf{0} & \cdots & \mathbf{0} & \mathbf{0} & \mathbf{E}_1^{\mathrm{H}} \\ \mathbf{0} & l\mathbf{K}_2 & \mathbf{0} & \cdots & \mathbf{0} & \mathbf{0} & \mathbf{E}_2^{\mathrm{H}} \\ \mathbf{0} & \mathbf{0} & l\mathbf{K}_3 & \cdots & \mathbf{0} & \mathbf{0} & \mathbf{E}_3^{\mathrm{H}} \\ \vdots & \vdots & \vdots & \ddots & \vdots & \vdots & \vdots \\ \mathbf{0} & \mathbf{0} & \mathbf{0} & \mathbf{0} & l\mathbf{K}_j & \mathbf{0} & \mathbf{E}_j^{\mathrm{H}} \\ \mathbf{0} & \mathbf{0} & \mathbf{0} & \mathbf{0} & \mathbf{0} & \mathbf{K}_{\mathrm{FE}} & \mathbf{C}_2^{\mathrm{T}} \\ \mathbf{E}_1 & \mathbf{E}_2 & \mathbf{E}_3 & \cdots & \mathbf{E}_j & \mathbf{C}_2 & \mathbf{R} \end{bmatrix} \tag{25}$$

where $\mathbf{K}_1, \mathbf{K}_2, \ldots, \mathbf{K}_j$ are small, banded, Hermitian matrices; $\mathbf{K}_{\mathrm{FE}}$ is a larger, banded, symmetric matrix; and $\mathbf{R}$ is a square matrix which is initially null but is modified to become a dense Hermitian matrix during the Gauss elimination.

For an example where the exact strip region has 6 nodes, each of $\mathbf{K}_1, \mathbf{K}_2, \ldots, \mathbf{K}_j$ has order 12×12, so that if $j = 12$ the matrix $\mathbf{K}_{\mathrm{GV}}$ in Eq. (23) has order 144×144. For a 20×20 FE mesh, the FE region has 441 nodes and $\mathbf{K}_{\mathrm{FE}}$ has order 1323×1323. The constraints required to enforce the end conditions and to equate the degrees of freedom at the boundaries between the regions give $\mathbf{R}$ an order of 82×82, so that $\mathbf{K}_{\mathrm{VFM}}$ has order 1549×1549. This is little more than the order of $\mathbf{K}_{\mathrm{FE}}$, so if the damaged region is small the matrix to be triangulated is considerably smaller than that required for a finite element analysis of the whole plate. Predictions from [35] indicate that analysis by VFM is typically around 4 times faster than a full finite element analysis.

Computational efficiency can therefore be greatly increased by storing and processing the different components of $\mathbf{K}_{\mathrm{VFM}}$ separately as in [39]. Only terms on and above the leading diagonal need to be stored and processed. The Gauss elimination procedure can be regarded as a matrix transformation without row interchanges. First, triangulating $l\mathbf{K}_1$, each pivotal element of $l\mathbf{K}_1$ is used to modify other elements in $l\mathbf{K}_1$; the pivotal element and related elements of $l\mathbf{K}_1$ and $\mathbf{E}_1^{\mathrm{T}}$ are used to modify $\mathbf{E}_1^{\mathrm{T}}$; elements of $\mathbf{E}_1^{\mathrm{T}}$ are then used to modify $\mathbf{R}$. During the transformation of $l\mathbf{K}_1$ and $\mathbf{E}_1^{\mathrm{T}}$, there are no changes to the other stiffness matrices and

constraint matrices. The same procedure is repeated for $l\mathbf{K}_2, \ldots, l\mathbf{K}_j$ and $\mathbf{E}_2^{\mathrm{T}}, \ldots, \mathbf{E}_j^{\mathrm{T}}$, and then for $\mathbf{K}_{\mathrm{FE}}$ and $\mathbf{C}_2^{\mathrm{T}}$. Finally, the pivotal elements of $\mathbf{R}$ are used to modify other elements in $\mathbf{R}$.

5. Numerical results

The hybrid method VFM, initially proposed by Suliman et al. [35] for delamination in composite plate, is extended in this paper to model an arbitrary cracked plate. The method can be applied to plates with arbitrary boundary conditions, provided the longitudinal ends $x = 0$ and $x = l$ are supported identically for consistency with the infinitely long EFM model of [39].

Table 1. List of cases considered.

Figure	Crack type	Crack location (x, y)	Method	FE region (y)	Mesh size (x, y)	Reference
4(a)	ATLC PTDC	Start (0,0.05) End (0.1,0.05)	VIPASA	-	2 strips	-
			VFM	0.035 to 0.065	20×10	
4(b)	ATLC PTDC	Start (0,0.075) End (0.1,0.075)	VIPASA	-	2 strips	-
			VFM	0.025 to 0.075	20×10	
7, 8	PTLC PTDC	Centre (0.05,0.05) *y* direction	AT	0 to 0.1	20×20	[8], [9], [10]
			ATCS	0 to 0.1	20×20	
			VFM	0.035 to 0.065	20×10	
			AFE	0.035 to 0.065	Varies	
9	PTLC ATDC	Start (0.05,0.1) *y* direction	AT	0 to 0.1	20×20	[11]
			ATCS	0 to 0.1	20×20	
			VFM	0.035 to 0.065	20×10	
10	PTLC ATDC	Start (0.075,0.1) *y* direction	AT	0 to 0.1	20×20	[11]
			ATCS	0 to 0.1	20×20	
			VFM	0.025 to 0.075	20×10	
13	ADC ATDC	Start (0.1,0.075) Various directions	VFM	0.025 to 0.075	20×10	-

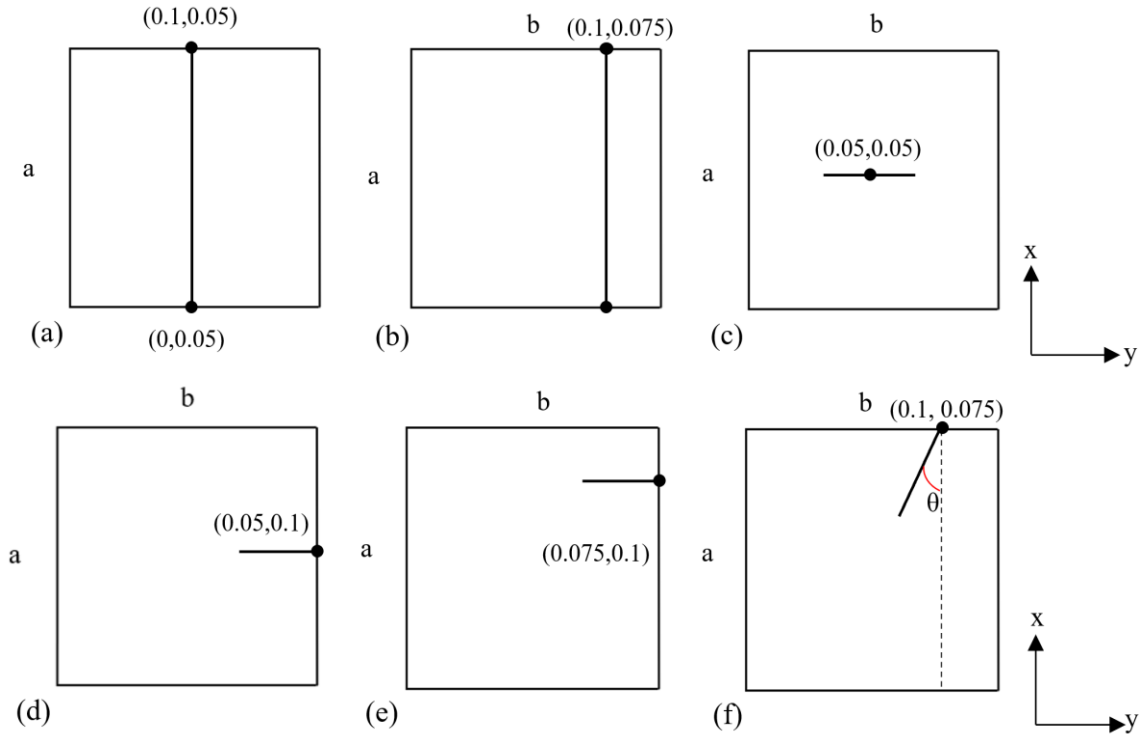

Fig. 3. Geometry and dimensions of a simply supported square plate with a crack at different locations (m). (a) ATLC located at the centre; (b) ATLC located 75% of the way along edge b; (c) PTLC located at the centre; (d) PTLC starting from the centre of edge a; (e) PTLC starting 75% of the way along edge a; (f) ADC at an angle θ starting 75% of the way along edge b.

For validation purposes, an isotropic simply supported plate is assumed and results obtained from VFM are compared with different modelling approaches: the ESM software VIPASA, the FE software ABAQUS [43] and various results from the literature. The dimensions and properties of the plate studied (Fig. 1) are defined as: Young's modulus $\mathrm{E} = 110 \times 10^9 \mathrm{Nm}^{-2}$; density $\rho = 4480 \mathrm{kgm}^{-3}$; Poisson's ratio $\nu = 0.3$; plate length $a = 0.1\mathrm{m}$; plate width $b = 0.1\mathrm{m}$; plate thickness $h = 10^{-3}\mathrm{m}$ and crack depth d. Different types of crack are discussed, as listed in Table 1 and Fig. 3, including: an all through-the-length crack (ATLC); a parallel part through-the-length crack (PTLC) and an arbitrary direction crack (ADC). The effects of structural damping and the loss of mass around the crack are ignored. Nondimensional frequency parameters are used for convenience

$$\bar{\omega}_j = 2\pi\omega_j * b^2 * \sqrt{\rho h / D} \tag{26}$$

where ω_j is the j^{th} natural frequency (Hz). The mode shapes will be identified in terms of (m, n), the number of half-waves in the x and y directions for the intact plate. The relative change in natural frequency (RCNF) is expressed as

$$\delta_j = (\overline{\omega_{0J}} - \overline{\omega}_j) \,/\, \overline{\omega_{0J}} \tag{27}$$

where $\overline{\omega_{0J}}$ is the j^{th} natural frequency of the intact plate.

5.1 All through-the-length crack (ATLC)

In the first crack problem shown in Fig. 3(a) and (b) the crack runs along the entire length of the plate. The damaged plate therefore retains its prismatic status in the longitudinal direction and can therefore be modelled using VIPASA for comparison with the hybrid VFM model for ATLCs at different locations and with varying crack depth. In the VIPASA model the plate is divided into two strips connected by a rotational spring to represent the crack. In the VFM model, the FE part is divided into 20×10 equally sized elements coupled with the two strips of the ESM at its edges by Lagrangian multipliers. Each of the ESM sections is 0.035m wide when the crack is in the centre and 0.025m when the crack is 75% of the way along the edge. Two point supports are added on each strip to model the simply supported ends.

Fig. 4 compares the results for isotropic plates having all through-the-length cracks located either at the centre or three quarters of the way along the edge of the plate. The same rotational spring model is used in both VIPASA and VFM. The mode shape for mode (1,2) is antisymmetric about the crack direction, so the curvature is zero if the crack is located along the centre line of the plate. Hence, the RCNF remains zero as shown in Fig. 4(c) for a crack location of $y = 0.05\text{m}$. Figs. 4 (a) to (c) show a good match between VICON and VFM when the crack occurs at different locations with varying depth ratios (*d/h*), the maximum difference being 1.02% when the depth ratio is 1. The main reason for the difference is the increasing element size used in the finite element portion of the VFM model. For the VFM model, the additional rotational spring stiffness are discretised to the nodes in the cracked elements, whereas in VIPASA they are continuous. A coarser mesh will then cause a more significant difference with the actual data when the severity of the crack increases.

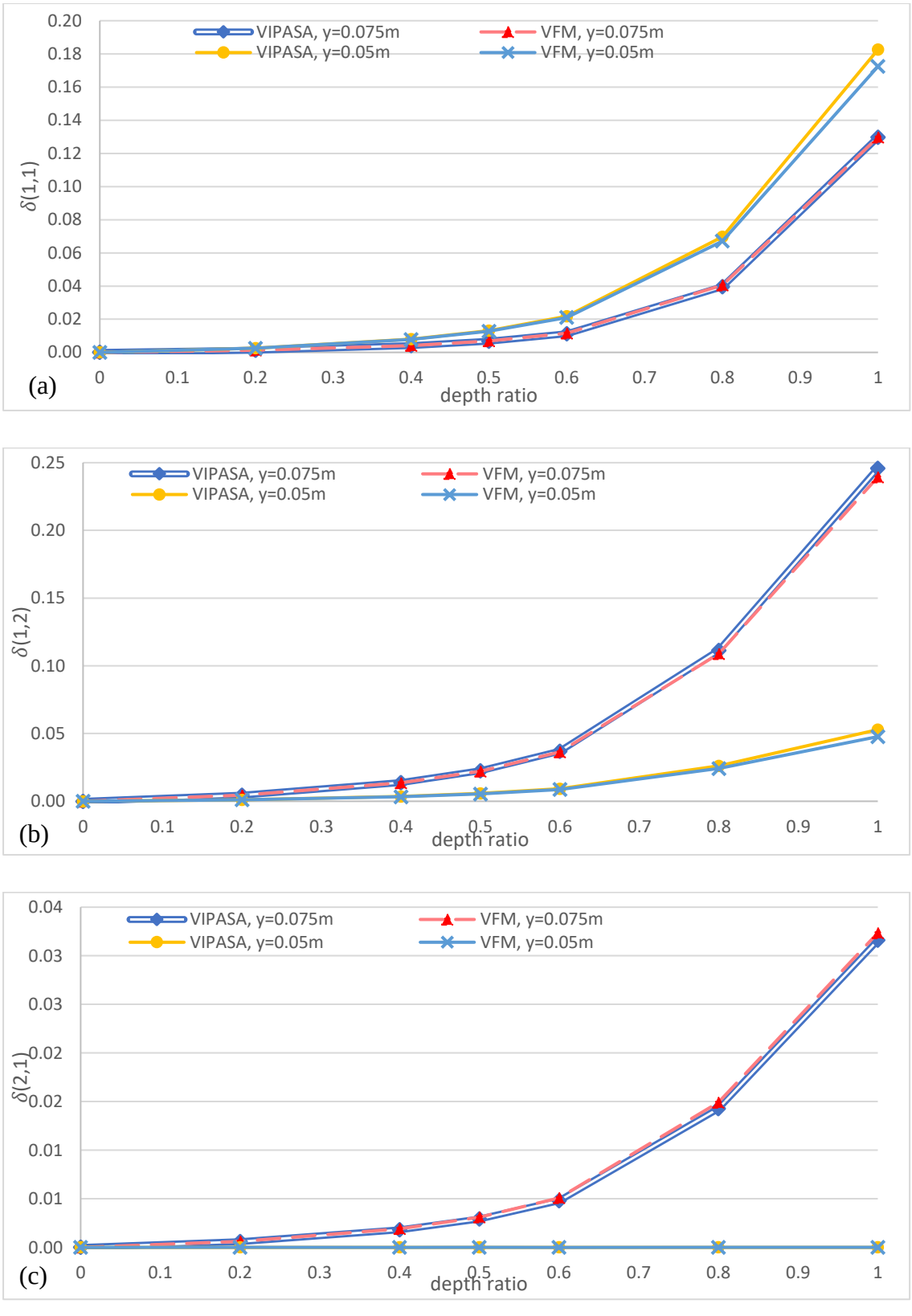

Fig. 4. Relative changes in the first three natural frequencies $\bar{\omega}_j$ of an isotropic plate against depth ratio *d/h* of an ATLC using VIPASA and VFM with different locations. (a) mode (1,1); (b) mode (1,2); (c) mode (2,1).

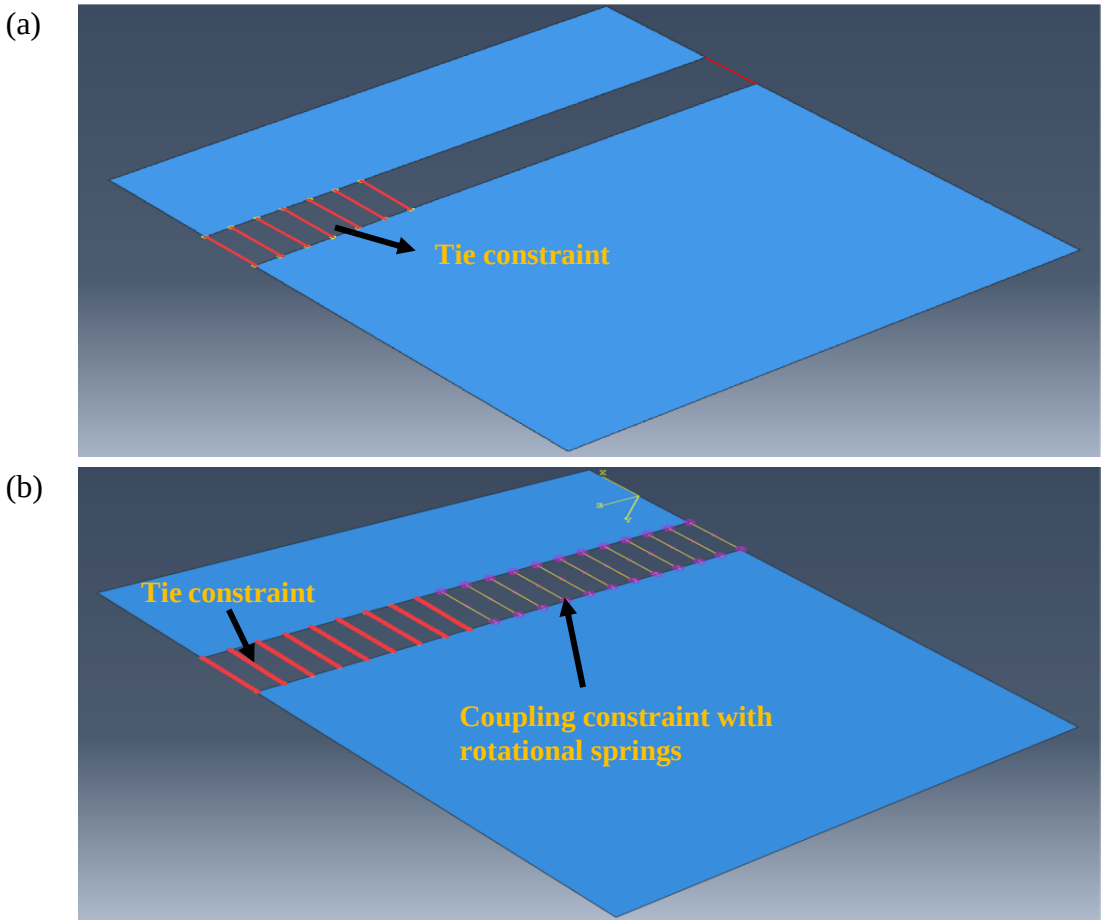

Fig. 5. ABAQUS models used in PTLC case. (a) AT; (b) ATCS.

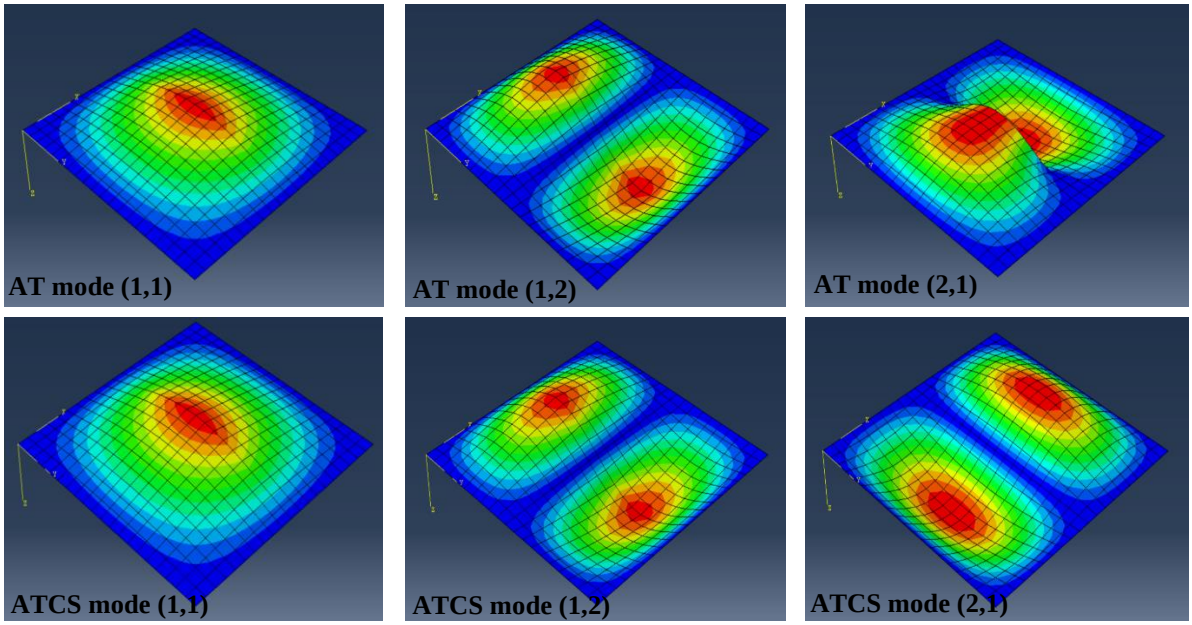

Fig. 6. Mode shape comparison between AT and ATCS for centrally located PTLC with length ratio 0.6.

5.2 Partial through-the-length crack (PTLC)

For partial through-the-depth and arbitrarily located cracks, relevant studies are largely absent from the literature. For partial through-the-length cracks (PTLC), cases that can be compared with the literature are all through-the-depth cracks starting from different locations with varying length ratios (l_c/b). Fig. 3 (c), (d) and (e) show the start point of each crack case. Because PTLC makes the plate non-prismatic, VIPASA cannot be used for the analysis. Hence, the PTLC case is validated against previous studies [8, 9, 11].

In order to verify the VFM model in more complicated cases, two ABAQUS models are introduced for further verification. These models use 4-node doubly thin curved shell S4R elements with six degrees of freedom at each node. Because only the first few natural frequencies are studied, only out-of-plane behaviour is considered, and the in-plane degrees of freedom are suppressed in the ABAQUS models. Hence, the model can be regarded as equivalent to VFM. A mesh of 400 equally sized square elements is used. The crack is simulated using two separate plates whose boundaries lie along the line of the crack (Fig. 5). Tie constraints are then used to constrain all six degrees of freedom in the non-cracked regions to ensure the two plates deform together. Two types of crack are simulated: all through the depth (ATD) and partial through the depth (PTD). The AT model (ABAQUS tie constraint only model) shown in Fig. 5(a) is used to match previous ATD studies. In the intact parts along the virtual crack line, relative movements are constrained at the boundary using tie constraints, but in the cracked region the two portions are able to move freely with respect to each other. For PTD studies, the ATCS model (ABAQUS with tie, coupling and rotational spring constraints) shown in Fig. 5(b) incorporates an additional rotational spring to simulate the crack in the damaged region. Tie constraints are still used in the intact parts. But in the cracked region, coupling constraints restrain all displacements and rotations, except for rotation about the crack direction. A rotational spring is then added [26, 32] to simulate the degraded stiffness of the damaged plate. Mode shapes from the two ABAQUS models are compared in Fig. 6.

Fig. 7 shows the relative changes in natural frequency for a centrally located ATD PTLC with varying length ratios. Comparison is made between results from VFM, ABAQUS and previous studies. Figs. 7 (a) and (b) show a small reduction in natural frequencies with increasing crack severity for symmetric modes in which the rotations dominate the vibration response behaviour in the damaged region and the out-of-plane displacement has a smaller effect. This reduction

is reflected in the mode plots in Fig. 6. Even when the crack penetrates through the length and depth of the plate, the maximum decrease for symmetric modes is only 20%. When the length ratio of an ATD crack is smaller than 0.4, the average reduction in natural frequencies is no more than 10%. A good agreement is seen in the plots of RCNF for all modes, with maximum differences of 2.48% and 0.71% for a length ratio of 0.4 for the first two natural frequencies, respectively. When an ATD crack penetrates the whole length of the plate, the difference in the values of RCNF is noticeable when comparing VFM with other studies because the out-of-plane displacement in the damaged part will dominate the behaviour of the vibration response when the ATDC is severe enough. If the displacement degrees of freedom are considered (which they are not in the VFM model), changes in natural frequencies are more significant, particularly for modes that are antisymmetric about the crack direction (e.g. the AT mode (2,1) in Fig. 6). However, when only the rotational degrees of freedom are considered, the natural frequencies of antisymmetric modes remain constant (e.g. the ATCS mode (2,1) in Fig. 6 and the PTLC mode (2,1) in Fig. 7) with increasing length of crack as in the ATLC cases.

Another reason for the discrepancy between results is caused by the increasing size of the simulated damaged region of the finite element part of the VFM model [35]. Since the current VFM model uses a fixed number of finite elements, the mesh becomes coarser with increasing width of the FE portion of the model, hence causing a loss of modelling accuracy. To investigate the influence of the number of elements used in the FE portion, a pure FE cracked plated model (AFE) was extracted from the VFM damaged region to compare with Liew et al.'s model [9] of the whole plate structure. As expected, Fig. 8 shows a better match with AFE and [9] when more finite elements are used to model the plate. For AFE 20×20 , the mesh comprises 400 elements equally distributed in the two directions. For AFE 40×40 , a finer mesh is used containing 1600 elements. Compared with the results presented in [9], differences in RCNF are 1.87% and 0.96% for AFE 20×20 and AFE 40×40, respectively. The accuracy of the results obtained from the finer mesh increase by just 0.91% while the computational time is 50 times that for 20×20. Balancing the computational efficiency and the accuracy of the results, AFE 20×10 is therefore chosen in the FE portion of the VFM model, which has the same effect on accuracy as when AFE 20×20 is used to model the whole plate.

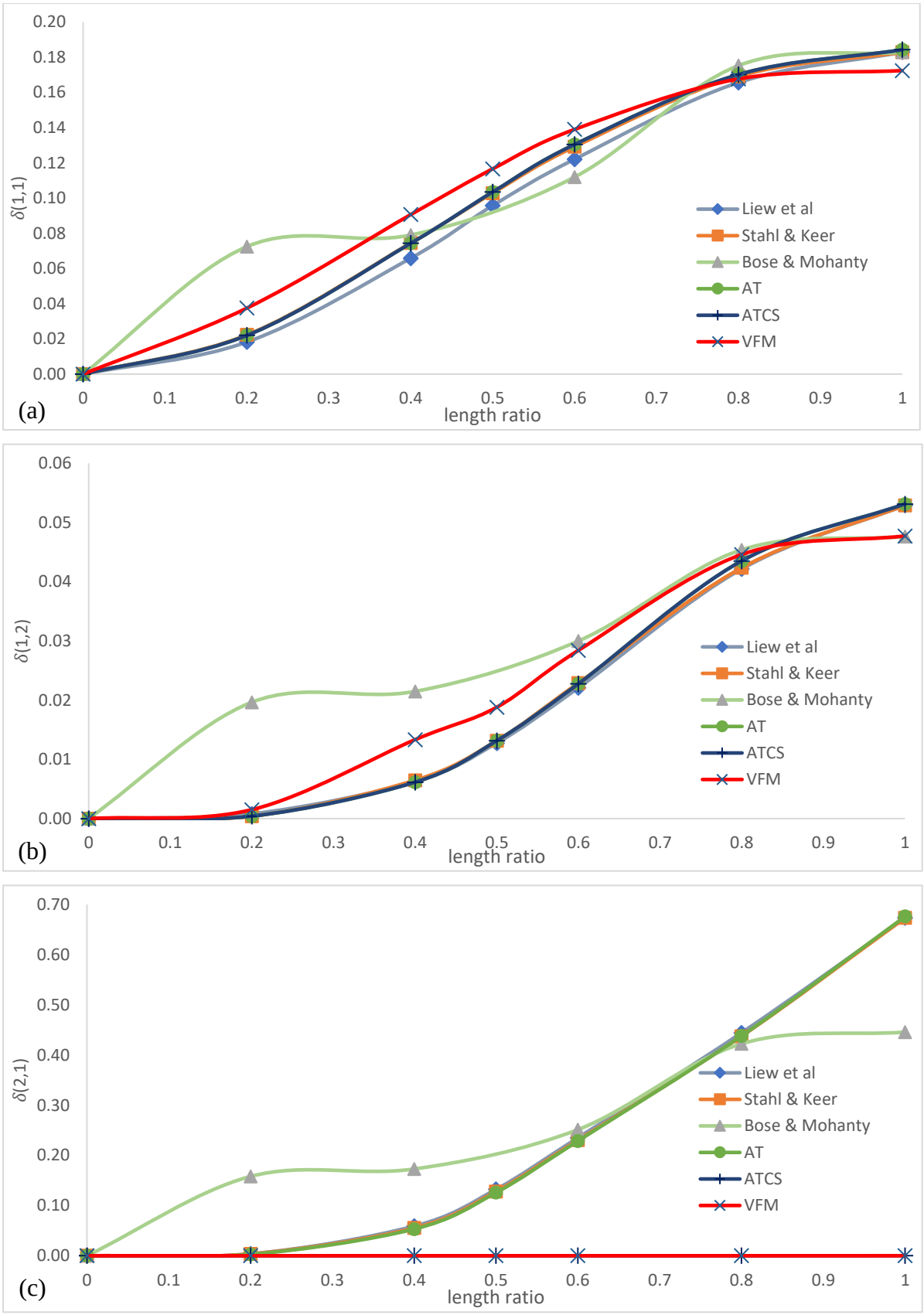

Fig. 7. First three RCNF vs length ratio for a centrally located PTLC using VFM, ABAQUS and previous methods [8-10]. (a) mode (1,1); (b) mode (1,2); (c) mode (2,1).

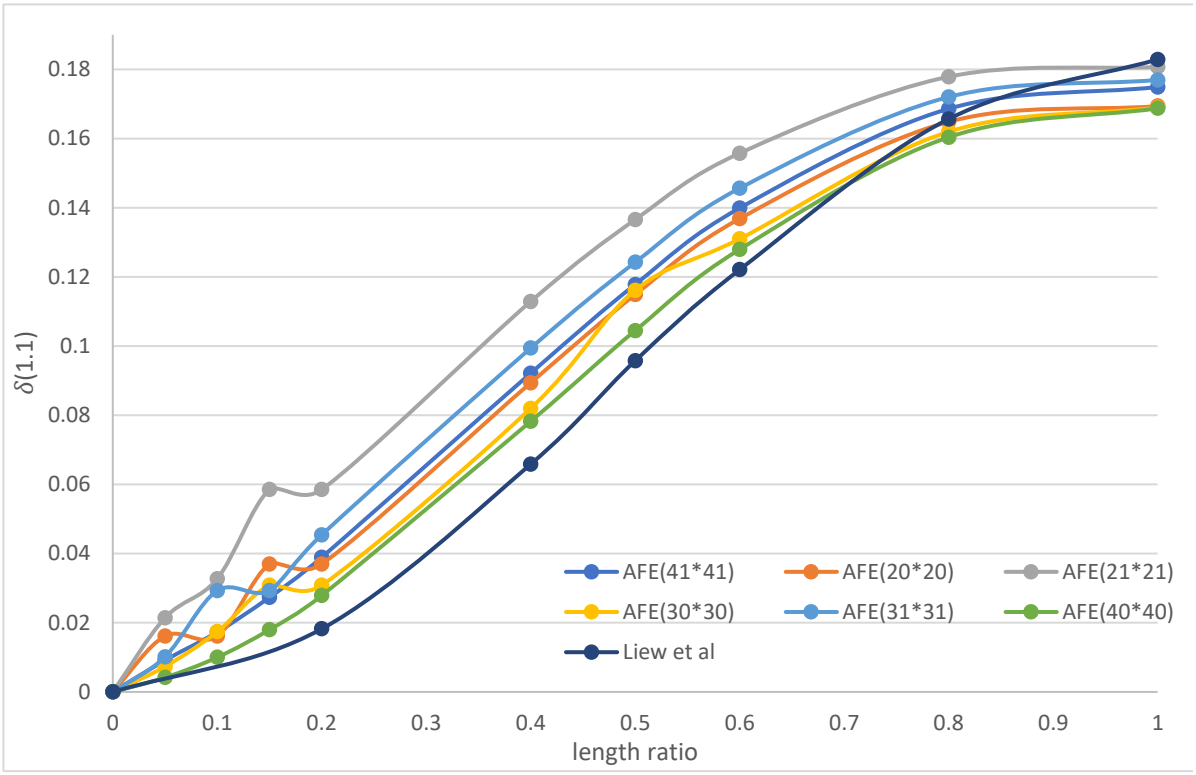

Fig. 8. Fundamental RCNF for centrally located ATD PTLC, using AFE model with various mesh sizes compared with Liew et al. [9].

A perturbation is seen in Fig. 8 for specific length ratios when changing the size of the elements. Coarser meshes are seen to result in larger perturbations particularly when the ATD crack is located within an element instead of at its edge. This is due to the way the rotational compliance is allocated in the FE portion of the model. When assembling the global stiffness matrix, the additional compliance induced by the crack is distributed to the corresponding nodes by integration of the shape function. If the crack is ATD, this compliance is infinite, causing zero rotational stiffness to be added to all four nodes of the element when the crack passes anywhere within an element, even if only for a short distance. Thus a higher reduction in natural frequencies will occur compared with when the crack ends exactly at the edge of the element. This perturbation phenomenon only occurs in the ATD case. In the PTD case the rotational compliance is finite and a smooth RCNF curve will be generated, but again accuracy is improved by using a finer mesh.

Fig. 7 presents a good match between the AT model and previous studies, as well as the between the ATCS model and the VFM model. Particularly for antisymmetric modes about the

crack direction, the ATCS model shows an entirely satisfactory agreement with the VFM model proving the equivalence of these two models. Hence, the ATCS model can now be used to analyse and compare more complicated cracked cases with the VFM model because there is an absence of previous PTD crack studies. Since the aim of damage identification is to detect a crack in its early stages, being able to model PTD cracks is essential.

Figs. 9 and 10 show a comparison of different results for PTLC starting from different edge points: namely the mid-point and the 75% point of edge a, see Figs. 3 (d) and (e). The crack runs parallel to the y axis and the first three lowest natural frequencies are considered. Fig. 9 shows similar degradation of the RCNF with the crack starting from the mid-point. Any difference is believed to be due to the increasing size of the simulated damaged region corresponding to the FE part of the VFM model. Care must be taken when interpreting the results of Huang and Leissa [11]. When the crack length ratio reaches 0.4, modes (1,2) and (2,1) are interchanged in their results because the authors recorded the sequence of the different modes based on the magnitude of their natural frequencies. With increasing crack severity, there is a sharp reduction in the differences in the natural frequencies of some modes while for others this change only occurs gradually. When an ATD crack starts from the middle of the plate, the results obtained in [9] show that the natural frequency of mode (2,1) reduces much faster than that of mode (1,2). This interchange has also been made in Fig. 11.

Fig. 10 illustrates the RCNF of a crack starting from the 75% point of edge a. Good agreement is shown between AT and [11], but there is an obvious difference between the results obtained from the VFM model in comparison to them. Again, this is caused by their different crack modelling assumptions and the increasing size of the cracked element in the FE portion of VFM model.

From Fig. 10, it is evident that the results obtained from the AT model match well with Huang and Leissa [11] while results from the ATCS model agree well with VFM. The main reason for this is again based on the modelling assumptions. Only mode (1,2) shows a good match for all four models across the full range of crack lengths. However, all the RCNF data matches well when the crack length ratio is smaller than 0.3. This difference in behaviour is also reflected in the mode shapes.

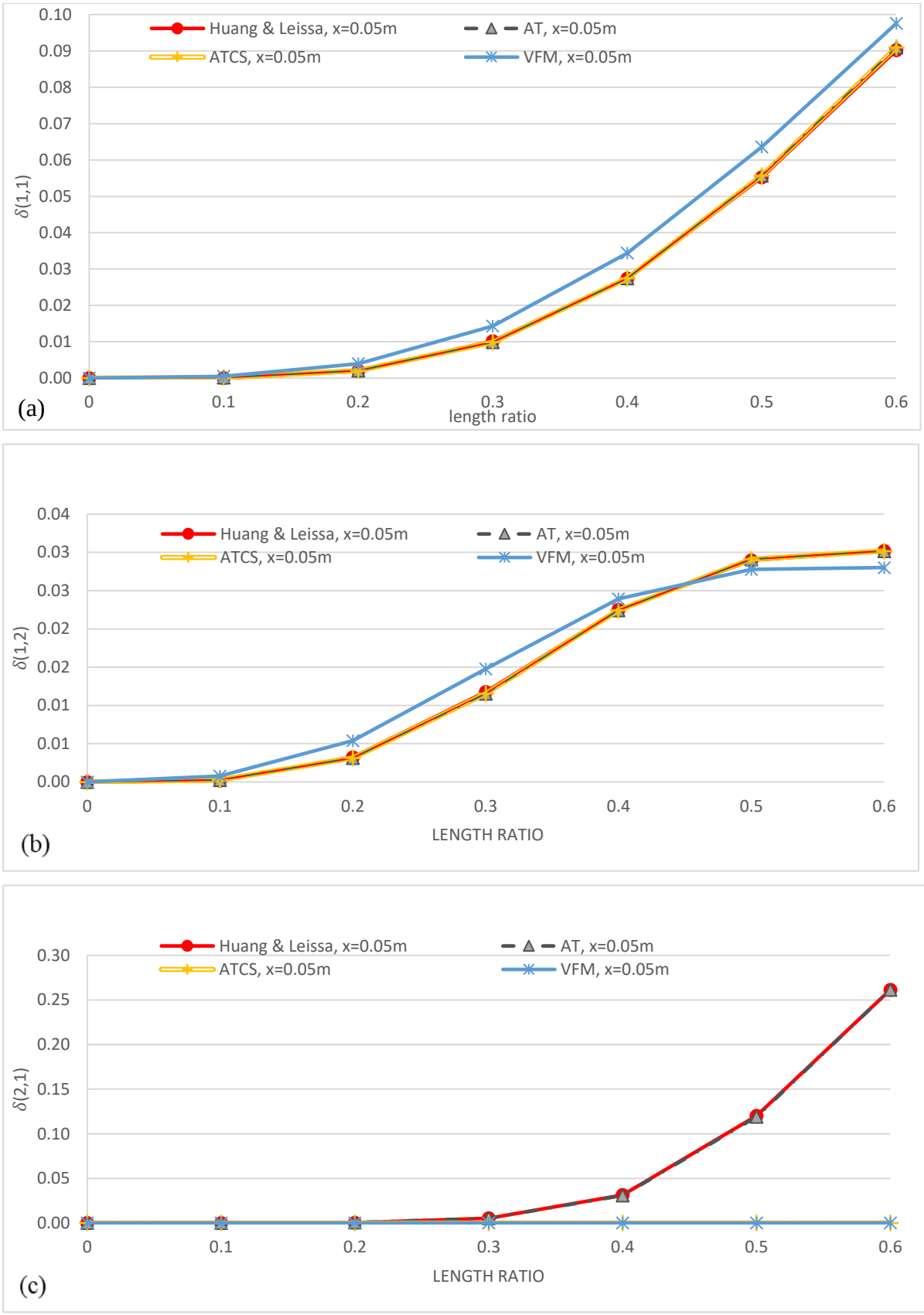

Fig. 9. First three RCNF vs. length ratio for PTLC starting from the centre of edge a, using VFM, ABAQUS and Huang and Leissa [11]. (a) mode (1,1); (b) mode (1,2); (c) mode (2,1).

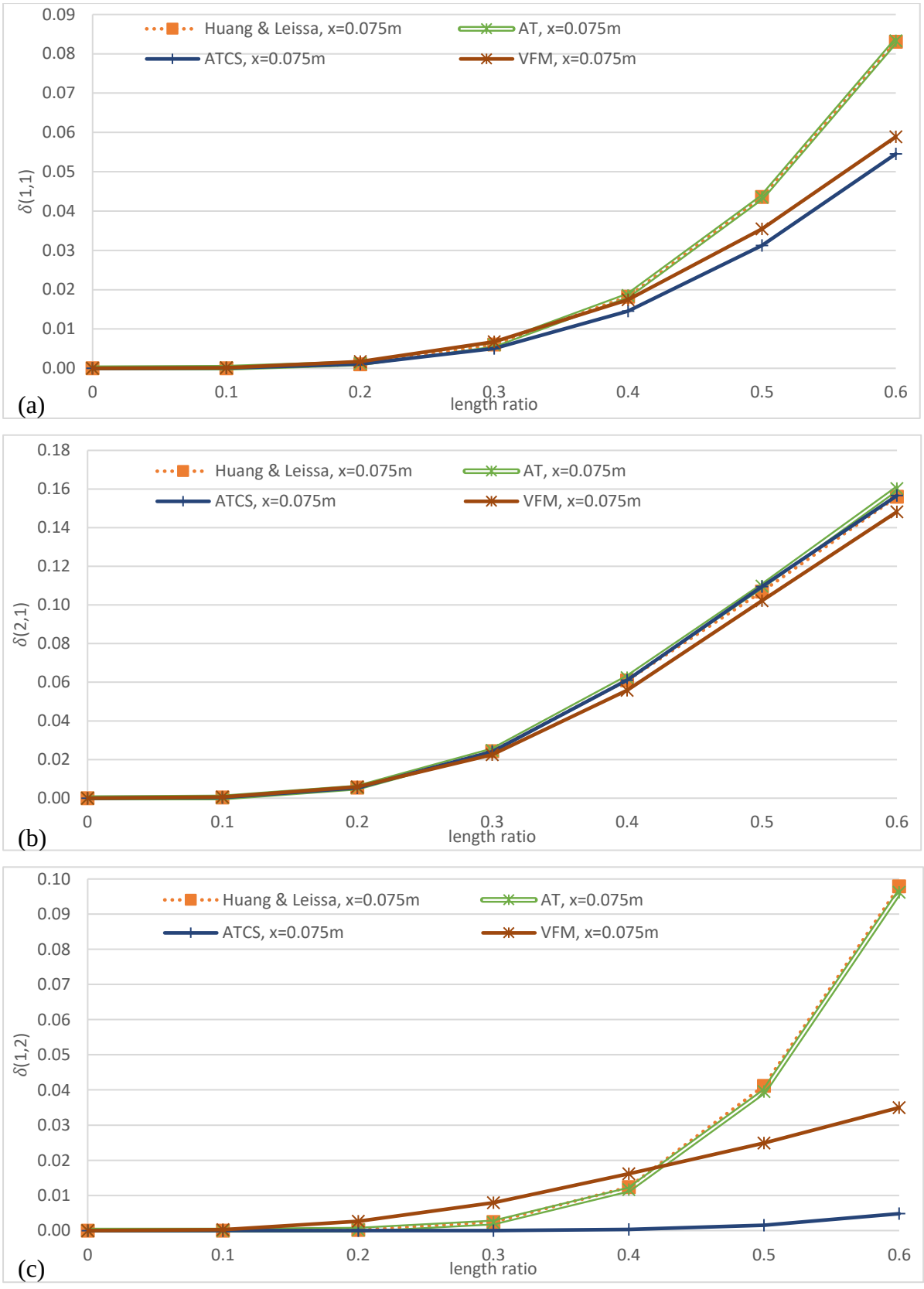

Fig. 10. First three RCNF vs. length ratio for PTLC starting 75% of the way along edge a, using VFM, ABAQUS and Huang and Leissa [11]. (a) mode (1,1); (b) mode (2,1); (c) mode (1,2).

Length ratio	Mode (1,2)		Mode (2,1)	
0.2	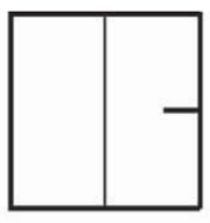	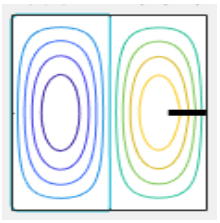		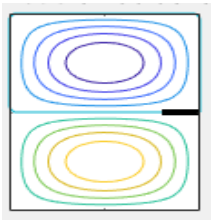
0.5	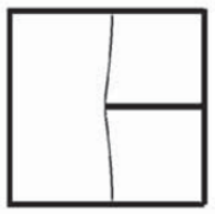	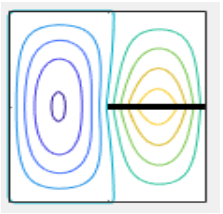	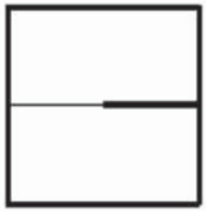	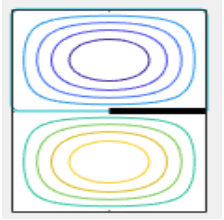
	(a) Huang and Leissa [11]	(b) VFM	(c) Huang and Leissa [11]	(d) VFM

Fig. 11. Mode shape comparison between VFM and Huang and Leissa [11] for PTLC starting from the centre of edge a.

Length ratio	Mode (1,1)	Mode (2,1)	Mode (1,2)	Mode (2,2)	Mode(3,1)
[11] 0.2				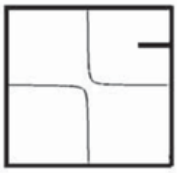	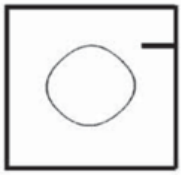
[11] 0.5					
VFM 0.2	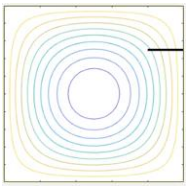	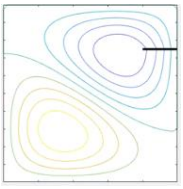	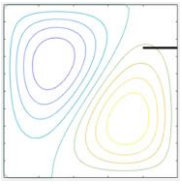	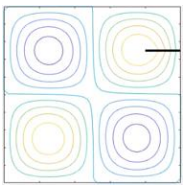	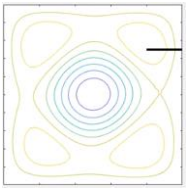
VFM 0.5	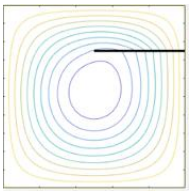	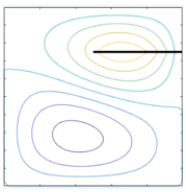	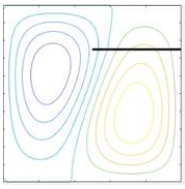	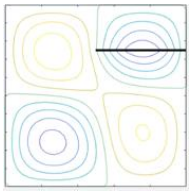	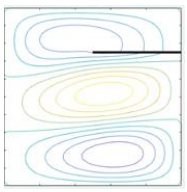

Fig. 12. Mode shape comparison between Huang and Leissa [11] and VFM, for PTLC starting 75% of the way along edge a.

As shown in Fig. 12, mode shapes reproduced from [11] show similar trends to the mode shapes plotted by VFM for a short crack. With increasing crack length ratio, the mode shapes from different models become more dissimilar. Even after accounting for mode interchanges (as in Fig. 11), a reason for this discrepancy is due to the crack simulation method causing a difference in mode shapes: VFM adopts only a rotational spring to simulate the crack while other approaches consider discontinuities in the out of plane displacement across the damaged region. For small cracks this effect is not significant, so the use of rotational springs is shown to be valid for simulation and can be extended to the PTD crack and ADC cases.

5.3 Arbitrary direction crack (ADC)

In the previous sections ATLC and PTLC have been analysed using VFM and the results compared with other approaches, for verification. However, in reality most cracks are not parallel to the edges of the plate and randomly located cracks with various shapes, directions and lengths will occur in plate structures. Few methods possess the ability to analyse such arbitrary cracks with random direction, length, location and depth. VFM provides an attractive method to simulate an arbitrary direction crack (ADC), by retaining a rectangular mesh in the FE region and simply adding rotational degrees of freedom to the existing nodes. In this paper the particular case of cracks starting from 75% of the way along the edge of a simply supported square isotropic plate as shown in Fig. 3(f) are studied. A number of cases, all with the same start point but with 0°, 15°, 30°, 45° crack angles, length ratios in the region (0.1, 0.6) and a depth ratio of 0.9999 are studied and the RCNFs from the first three modes are plotted in Fig. 13. Because the crack is not symmetrically located, the behaviour is unsymmetrical even for a square plate. The frequencies are all affected by the crack direction, larger changes occurring as the crack reaches regions of high curvature in the mode shape. Thus the changes do not vary monotonically with θ. For example, for the first two natural frequencies in Figs. 13 (a) and (b), more significant changes occur when $\theta \neq 0°$. However, because of the methods of crack simulation and assignment of the additional spring stiffness mentioned above, when an ATD crack cannot start and finish at the element edge, the changes in natural frequencies are higher than expected. The mesh of the element also affects the RCNF resulting in a perturbation curve similar to that in Fig. 8.

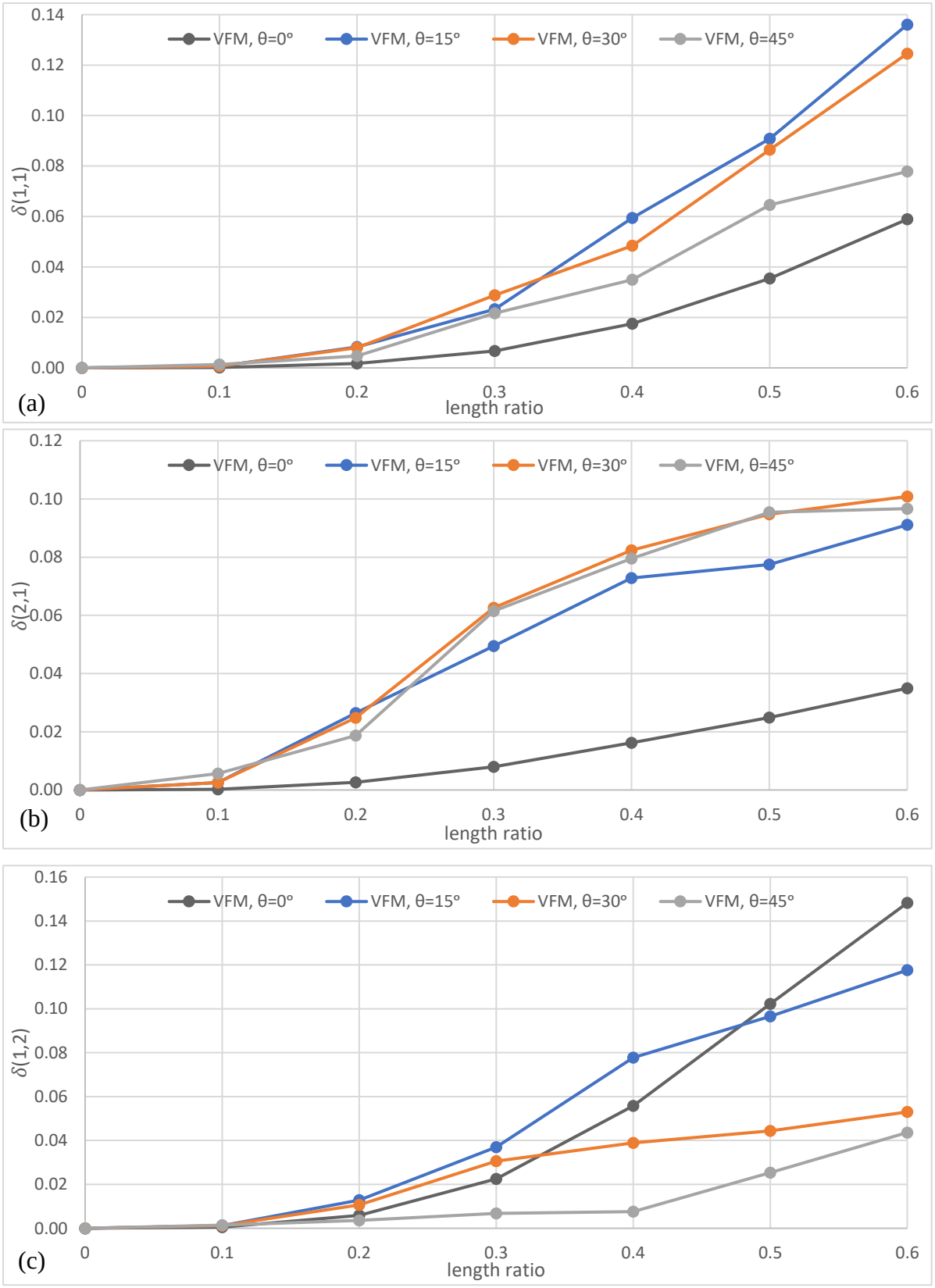

Fig. 13. First three RCNF vs. length ratio for ADC starting 75% of the way along edge b with different crack angles, using VFM. (a) mode (1,1); (b) mode (2,1); (c) mode (1,2).

6. Conclusions

This paper presents a novel method for the simulation of cracks with arbitrary location, depth, length and orientation in plate-type structures. A cracked plate model was developed based on the equivalent dynamic stiffness matrix of the FE model programmed in MATLAB with additional degrees of freedom added to represent the crack. The method allowed the crack to pass through any part of an element by simulating it as a rotational spring resolved about the longitudinal and transverse axes using shape functions, before assigning these rotational spring stiffnesses to the corresponding nodes of the element to generate the global stiffness matrix of the cracked plate structure. A hybrid model was then assembled by coupling an exact strip model for the undamaged parts of the plate with this FE model for the damaged part using Lagrangian multipliers to equate the deflections and rotations at the boundaries. The Wittrick-Williams algorithm was applied to obtain the natural frequencies to any required accuracy whilst avoiding missing any values. For the simply supported isotropic square plate used in this study, only the out-of-plane behaviour is considered and the first three natural frequencies are discussed for comparison. Hence, a modified Wittrick-Williams algorithm was utilised without the need to consider the effect of fixed-end natural frequencies. A banded Gauss elimination method was used to achieve a significant saving of computational cost whilst maintaining an acceptable calculation accuracy. Furthermore, by using the newly proposed crack simulation method, remeshing was avoided by introducing additional degrees of freedom at the nodes of the cracked elements.

The proposed hybrid model has been validated against previous studies and corresponding ABAQUS models. Different types of crack were modelled and their effects on the vibration response of the plate were compared. Due to the limitations created by utilising classical plate theory for the FE portion [35] and using only rotational springs to simulate the crack, changes in natural frequencies were selected as the variable to be compared. An acceptable difference (smaller than 3%) was shown in the results between the predictions of changes in natural frequencies and those found in the literature. This showed a good match for the hybrid model even when the crack was severe. Due to the crack simulation and symmetry of the structure, lines of zero curvature exist for some modes, for example when the crack occurs at the centre of plate. If the crack runs along one of these lines, it has no effect on the local stiffness of the plate and the change in natural frequencies is zero. When the crack runs off-centre of the plate, it breaks this symmetry causing more significant effects such as changes in mode order. The

changes in natural frequencies were found to match well with previous studies when the length ratio was less than 0.4, but not when the crack became more severe. Therefore, when using the hybrid model with only a rotational spring based on fracture mechanics to simulate a crack, accuracy will be lost at high natural frequencies or when the crack severity is high, as noted in [44].

The hybrid approach combines the computational efficiency of the exact strip method with the versatility of finite element analysis. The proposed method can fill gaps in the literature for cracks with arbitrary length, depth, location and orientation. The hybrid cracked model is a useful extension of the delamination hybrid model proposed by Suliman et al. [35] and also a supplement for the exact strip method which could previously only be used for prismatic structures. Although only a simply supported square isotropic plate was considered in this study, the present verified methodology can be applied to rectangular plates with other aspect ratios and boundary conditions. Additional types of spring could also be introduced to simulate cracks in more general cases (e.g. incorporating out-of-plane displacement). The methodology could also be extended to analyse more complicated plate-type structures like stiffened panels and composites.

Acknowledgement

This work was support by China Scholarship Council (CSC).

References

[1] J.A. Escobar, J.J. Sosa, R. Gómez, Structural damage detection using the transformation matrix. Computers and Structures 83 (4–5) (2005) 357–368. doi: 10.1016/j.compstruc.2004.08.013.

[2] X. Fang, H. Luo, J. Tang, Structural damage detection using neural network with learning rate improvement. Computers and Structures 83 (25–26) (2005) 2150–2161. doi: 10.1016/j.compstruc.2005.02.029.

[3] M. Ge, E.M. Lui, Structural damage identification using system dynamic properties. Computers and Structures 83 (27) (2005) 2185–2196. doi: 10.1016/j.compstruc.2005.05.002.

[4] S. Caddemi, A. Greco, The influence of instrumental errors on the static identification of damage parameters for elastic beams. Computers and Structures 84 (26–27) (2006) 1696–1708.

doi: 10.1016/j.compstruc.2006.03.010.

[5] Z. Wang, K.C.G. Ong, Autoregressive coefficients based Hotelling's T^2 control chart for structural health monitoring. Computers and Structures 86 (19–20) (2008) 1918–1935. doi: 10.1016/j.compstruc.2008.02.007.

[6] E.N. Chatzi, B. Hiriyur, H. Waisman, A.W. Smyth, Experimental application and enhancement of the XFEM-GA algorithm for the detection of flaws in structures. Computers and Structures 89 (7–8) (2011) 556–570. doi: 10.1016/j.compstruc.2010.12.014.

[7] O.S. Salawu, Detection of structural damage through changes in frequency: a review. Engineering Structures 19 (9) (1997) 718–723. doi: 10.1016/S0141-0296(96)00149-6.

[8] B. Stahl, L.M. Keer, Vibration and stability of cracked rectangular plates. International Journal of Solids and Structures 8 (1) (1972) 69–91. doi: 10.1016/0020-7683(72)90052-2.

[9] K.M. Liew, K.C. Hung, M.K. Lim, A solution method for analysis of cracked plates under vibration. Engineering Fracture Mechanics 48 (3) (1994) 393–404. doi: 10.1016/0013-7944(94)90130-9.

[10] T. Bose, A.R. Mohanty, Vibration analysis of a rectangular thin isotropic plate with a part-through surface crack of arbitrary orientation and position. Journal of Sound and Vibration 332 (26) (2013) 7123–7141. doi: 10.1016/j.jsv.2013.08.017.

[11] C.S. Huang, A.W. Leissa, Vibration analysis of rectangular plates with side cracks via the Ritz method. Journal of Sound and Vibration 323 (3–5) (2009) 974–988. doi: 10.1016/j.jsv.2009.01.018.

[12] Y. Hirano, K. Okazaki, Vibration of cracked rectangular plates. Bulletin of JSME 23 (179) (1980) 732–740. doi: 10.1299/jsme1958.23.732.

[13] R. Solecki, Bending vibration of simply supported rectangular plates with internal rigid support. International Journal of Engineering Science 18 (11) (1980) 1309–1318. doi: 10.1016/0020-7225(80)90122-6.

[14] R. Solecki, Bending vibration of a simply supported rectangular plate with a crack parallel to one edge. Engineering Fracture Mechanics 18 (6) (1983) 1111–1118. doi: 10.1016/0013-7944(83)90004-8.

[15] G.L. Qian, S.N. Gu, J.S. Jiang, A finite element model of cracked plates and application to vibration problems. Computers and Structures 39 (5) (1991) 483–487. doi: 10.1016/0045-7949(91)90056-R.

[16] M. Krawczuk, Natural vibrations of rectangular plates with a through crack. Archive of Applied Mechanics 63 (7) (1993) 491–504. DOI: 10.1007/BF00788047.

[17] M. Krawczuk, A. Zak, W. Ostachowicz, Finite element model of plate with elasto-plastic through crack. Computers and Structures 79 (5) (2001) 519–532. doi: 10.1016/S0045-7949(00)00156-5.

[18] T. Fujimoto, K.Wakata, F. Cao, H. Nisitani, Vibration analysis of a cracked plate subjected to tension using a hybrid method of FEM and BFM. Materials Science Forum 440-41 (2003) 407–414. ISSN: 02555476.

[19] A. Saito, M.P. Castanier, C. Pierre, Estimation and veering analysis of nonlinear resonant frequencies of cracked plates. Journal of Sound and Vibration 326 (3–5) (2009) 725–739. doi: 10.1016/j.jsv.2009.05.009.

[20] C.S. Huang, A.W. Leissa, R.S. Li, Accurate vibration analysis of thick, cracked rectangular plates. Journal of Sound and Vibration 330 (9) (2011) 2079–2093. doi: 10.1016/j.jsv.2010.11.007.

[21] R. Ismail, M.P. Cartmell, An investigation into the vibration analysis of a plate with a surface crack of variable angular orientation. Journal of Sound and Vibration 331 (12) (2012) 2929–2948. doi: 10.1016/j.jsv.2012.02.011.

[22] R.Y. Liang, F.K. Choy, J. Hu, Detection of cracks in beam structures using measurements of natural frequencies. Journal of the Franklin Institute 328 (4) (1991) 505–518. DOI: 10.1016/0016-0032(91)90023-V.

[23] M.N. Cerri, F. Vestroni, Detection of damage in beams subjected to diffused cracking. Journal of Sound and Vibration 234 (2) (2000) 259–276. doi: 10.1006/jsvi.1999.2887.

[24] F. Vestroni, D. Capecchi, Damage detection in beam structures based on frequency measurements. Journal of Engineering Mechanics 126 (7) (2000) 761–768. doi: 10.1061/(ASCE)0733-9399(2000)126:7(761)

[25] M.I. Friswell, Damage identification using inverse methods. Philosophical Transactions of the Royal Society A: Mathematical, Physical and Engineering Sciences 365 (1851) (2007) 393–410. doi: 10.1098/rsta.2006.1930.

[26] A. Labib, D. Kennedy, C. Featherston, Free vibration analysis of beams and frames with multiple cracks for damage detection. Journal of Sound and Vibration 333 (20) (2014) 4991–5003. doi: 10.1016/j.jsv.2014.05.015.

[27] P.F. Rizos, N. Aspragathos, A.D. Dimarogonas, Identification of crack location and magnitude in a cantilever beam from the vibration modes. Journal of Sound and Vibration 138 (3) (1990) 381–388. doi: 10.1016/0022-460X(90)90593-O.

[28] W.M. Ostachowicz, M. Krawczuk, Analysis of the effect of cracks on the natural frequencies of a cantilever beam. Journal of Sound and Vibration 150 (2) (1991) 191–201. doi: 10.1016/0022-460X(91)90615-Q.

[29] A.D. Dimarogonas, Vibration of cracked structures: A state of the art review. Engineering Fracture Mechanics 55 (5) (1996) 831–857. doi: 10.1016/0013-7944(94)00175-8.

[30] T.G. Chondros, A.D. Dimarogonas, J. Yao, A continuous cracked beam vibration theory. Journal of Sound and Vibration 215 (1) (1998) 17–34. doi: 10.1006/jsvi.1998.1640.

[31] S. Caddemi, I. Caliò, Exact closed-form solution for the vibration modes of the Euler-Bernoulli beam with multiple open cracks. Journal of Sound and Vibration 327 (3–5) (2009) 473–489. doi: 10.1016/j.jsv.2009.07.008.

[32] S. Caddemi, I. Caliò, Exact solution of the multi-cracked Euler-Bernoulli column. International Journal of Solids and Structures 45 (5) (2008) 1332–1351. doi: 10.1016/j.ijsolstr.2007.09.022.

[33] W.H. Wittrick, F.W. Williams, A general algorithm for computing natural frequencies of

elastic structures. Quarterly Journal of Mechanics and Applied Mathematics 24 (3) (1971) 263–284. doi: 10.1093/qjmam/24.3.263.

[34] W.H. Wittrick, F.W. Williams, Buckling and vibration of anisotropic or isotropic plate assemblies under combined loadings. International Journal of Mechanical Sciences 16 (4) (1974) 209–239. doi: 10.1016/0020-7403(74)90069-1.

[35] B. Suliman, C.A. Featherston, D. Kennedy, A hybrid method for modelling damage in composites and its effect on natural frequency. Computers and Structures 213 (2019) 40–50. doi: 10.1016/j.compstruc.2018.12.003.

[36] J.R. Banerjee, Dynamic stiffness formulation for structural elements: A general approach. Computers and Structures 63 (1) (1997) 101–103. doi: 10.1016/S0045-7949(96)00326-4.

[37] W.H. Wittrick, General sinusoidal stiffness matrices for buckling and vibration analyses of thin flat-walled structures. International Journal of Mechanical Sciences 10 (12) (1968). 949–966. doi: 10.1016/0020-7403(68)90049-0.

[38] F.W. Williams, M.S. Anderson, Incorporation of Lagrangian multipliers into an algorithm for finding exact natural frequencies or critical buckling loads. International Journal of Mechanical Sciences 25 (8) (1983) 579–584. doi: 10.1016/0020-7403(83)90049-8.

[39] M.S. Anderson, F.W. Williams, C.J. Wright, Buckling and vibration of any prismatic assembly of shear and compression loaded anisotropic plates with an arbitrary supporting structure. International Journal of Mechanical Sciences 25 (8) (1983) 585–596. doi: 10.1016/0020-7403(83)90050-4.

[40] J.S. Przemieniecki, Theory of Matrix Structural Analysis, Dover, 2003. ISBN: 978-0486649481.

[41] A. Morassi, F. Vestroni, Dynamic Methods for Damage Detection in Structures. Springer, 2008. ISBN 978-3-211-78777-9.

[42] C.T. Hopper, F.W. Williams, Mode finding in nonlinear structural eigenvalue calculations. Journal of Structural Mechanics 5 (3) (1977) 255-278. doi: 10.1080/03601217708907314

[43] Dassault Systèmes, ABAQUS, version 6.12, (2013).

[44] W. Fan, P. Qiao, Vibration-based damage identification methods: a review and comparative study. Structural Health Monitoring 10 (1) (2011) 83–111. doi: 10.1177/1475921710365419.